DISTANCE PROTECTION CHALLENGES OF CONVERTER-INTERFACED RENEWABLE ENERGY SOURCES

AMIN BANAIEMOQADAMFARIMAN

A THESIS SUBMITTED TO THE FACULTY OF GRADUATE STUDIES
IN PARTIAL FULFILMENT OF THE REQUIREMENTS
FOR THE DEGREE OF

MASTER OF APPLIED SCIENCE

GRADUATE PROGRAM IN ELECTRICAL AND COMPUTER ENGINEERING
YORK UNIVERSITY
TORONTO, ONTARIO
AUGUST 2018

Abstract

Full-scale converter-interfaced renewable energy sources (CIRESs) can cause misoperation of distance relays installed in their vicinity. Such failure stems from the different fault behavior of CIRESs compared to synchronous generators (SGs), based on which existing relays have been developed. Several measures have been devised to improve the performance of distance protection by modifying existing relays. This thesis proposes a new approach to tackle this problem by regulating the CIRES's fault current such that available distance relays function properly, without requiring modification. The prime objective of this method is to mimic certain features of the symmetrical components of SGs' fault current while the constraints of a converter, such as its limited fault current magnitude, are satisfied. As a result, correct operation of distance relays close to CIRESs is ensured regardless of the fault characteristics, including its type, resistance, and location. Some salient features of the proposed method are its simplicity, compatibility with off-the-shelf relays, and independence from the voltage and power rating of the CIRES. Moreover, the proposed method uses only local measurements. Thus, no communication infrastructure is required, and so the proposed method is cost-effective. PSCAD/EMTDC simulation studies verify the performance of this new method.

Acknowledgements

I would like to express my sincere gratitude and appreciation to Dr. Hooshyar whose priceless support during the past two years paved my way toward becoming not only a researcher but a person with bigger dreams. He taught me how I should work hard to achieve my goals, how not to disappoint while being stuck in dead-ends of the research, how to think out-of-box, how to combine science with industry, and, more importantly, how to outrun myself.

I am honored that this dissertation has been examined by Dr. Rezaei and Dr. Gingerich. I owe respect and thanks to them for their time and consideration.

I would like to thank my office-mate, roommate, and the best friend Ahmad Olia for his unqualified support since the first day I came to Canada. He was the one who helped me overcome difficulties of immigrating to another country by the memorable moments we had together.

I also want to express my highest level of appreciation and gratitude to my parents who tried days and nights so that I have a comfortable life and can go after my dreams. I am far away from them, but they always have my heart.

Contents

List of Tables

List of Figures

Abbreviations

CIRES Converter-Interfaced Renewable Energy Source

SG Synchronous Generator

RES Renewable Energy Source

GC Grid Code

PV Photovoltaic

WF Wind Farm

HV High Voltage

LV Low Voltage

PF Power Factor

EU-GC European Grid Code

NA-GC North American Grid Code

PCC Point of Common Coupling

AG Phase-A-to-Ground

BCG Phase-B-to-Phase-C-to-Ground

ABG Phase-A-to-Phase-B-to-Ground

KVL Kirchhoff's Voltage Law

SLG Single-Line-to-Ground

LLG Line-to-Line-to-ground

LL Line-to-Line

DD Disturbance Detector

Chapter 1

Introduction

A fault is any failure which interferes with normal flow of current in a power system. Faults can happen due to different reasons such as equipment insulation fails due to system overvoltages caused by lightening or switching surges, insulation contamination, or other mechanical causes. In the case of fault, the current magnitude can reach up to several times larger than the normal current of the system. Such large currents, if not cleared fast, may cause thermal or mechanical damage to equipment. It is therefore vital to remove faulted sections of a power system from service as soon as possible. In a three-phase system, faults are categorized into two major types of balanced and unbalanced faults. Balanced faults include three-phase-to-ground faults. Unbalanced faults contain single-line-to-ground, line-to-line, line-to-line-to-ground, and three-phase faults [2,3]. Protective equipment in charge of detecting faults and taking proper actions to return the power system to its normal state are called relays [4].

The growing share of renewable energy sources (RESs) has led to a fault-ride-through require-

ment of modern grid codes (GCs) [5]. For example, by the year 2016, about 14000 Megawatts was the installed capacity of wind farms and photovoltaic solar panels in Canada, and also renewable energy sources provided 18% of the Canada's total electricity generation, which a significant amount [6]. As a result, a non-negligible portion of relay measurements during faults can arise from RESs. Meanwhile, existing relays are developed based on the assumption that generation units include only synchronous generators (SGs). However, the majority of RESs—such as solar photovoltaic (PV) and Type IV wind farms (WFs)—are coupled with the grid through a power electronic converter. The fault behavior of converter-interfaced RESs (CIRESs) is different from that of SGs, thus adversely affecting the performance of relays, especially those in close proximity of CIRESs, which are installed at the busbar connected to the CIRES or other neighboring busbars [7–9]. The increasing power rating of CIRESs aggravates this problem further. The control scheme used in a CIRES determines the characteristics of the fault current based on internal references or designated GCs [10]. Hence, unlike SGs, neither the magnitude nor the phase of the fault current is entirely dependent on the fault type and resistance and is regulated by the CIRES's control system and its references, generated by the GCs or manually.

Distance relays are used for both primary and backup protection in transmission systems [11]. Integration of CIRESs with the grid poses several challenges for distance protection. Misoperation of distance relays that protect the lines emanating from CIRESs has been investigated in [7]. In this paper, the performance of commercially available distance relays under various conditions has been assessed. Several cases were studied to investigate misoperation of distance relays for zone 1 and zone 2 faults, as the CIRES tries to comply with various GCs. For example, it is shown

that the impedance measured during a balanced fault with fault resistance of 10 Ω in zone 1 of a self-polarized distance relay installed at high voltage (HV) side of the transformer connected to the CIRES lies far beyond the trip zone, and the relay misoperates. During this fault, the CIRES meets the unity power factor (PF) requirement of European GC (EU-GC). Similar misoperations are also reported during other internal and external fault types. Finally, it is shown that the mioperations are caused due to the current source nature of CIRESs that negatively impacts both dependability and security of distance relays.

CIRESs also adversely affect the supervising elements of distance relays. For example, it is shown in [8] and [9] that the negative-sequence directional elements of the relays detect the fault direction incorrectly in the presence of CIRES. In [8], the relay installed at the collector bus of a Type IV WF mistakenly tripped the breaker for a fault on adjacent collector bus. Stored event data indicate that the negative-sequence directional element of the relay misidentified the fault direction, thereby declaring a reverse fault as a forward one. The misoperation is attributed to the converter's attempt to balance the current, and so minimize the negative-sequence component of the fault current.

To address some of the above problems, various solutions, including new impedance measurement relations and alternative modifications of the reactance element, were proposed for the phase and ground elements of distance relays in [9]. These solutions require several changes to the algorithms implemented by currently installed relays. This approach is feasible for future installations—in which upgraded distance relays can be used—, but not for existing installations.

To address maloperation of distance relays in the presence of CIRESs, another possible

solution is to use line current differential relays. However, this solution requires a high-bandwidth communication channel, which is costly. In addition, the communication channel can be prone to failure, in which case the distance element would govern the trip signal of the relay [12, 13]. More importantly, to address the uncertainties of the communication link, the trip logics applied by the utilities often combine the outputs of the line current differential and distance elements. For example, the trip logic defined by Hydro One, the transmission utility in Ontario, Canada, asserts the trip command during a pickup of the line current differential element only if it is accompanied by a zone 2 pickup of the distance element of the relay. Therefore, line current differential relays cannot be the ultimate solution to the above problems.

1.1 Research Objectives

One way to approach distance protection challenges of the relays in close proximity of CIRESs is the one practiced by existing remedies, discussed in the previous paragraph. The foundation of this approach is to modify relay elements, such as ground, phase, and directional elements, or design new relays such that they operate properly in the presence of CIRESs.

In this research work, a different approach to the above-mentioned problems is taken. Instead of modifying distance relays such that they operate properly in the presence of CIRESs, here, it is proposed that the fault behavior of CIRESs become as close as possible to that of SGs, based on which distance relays have been developed and operate properly. It is expected that the control system of the CIRES pave the way for reaping this objective, since the CIRES's control system regulates the current with respect to generated reference signals. Therefore, the fault behavior of

a CIRES including current magnitude and angle mainly depends on its control system. Hence, the main objective of this research work is to develop a new control scheme for CIRESs to address distance protection challenges caused in the presence of CIRESs.

1.2 Thesis Outline

This Thesis is organized as follows. In Chapter 2, the test system used for this study is described. Chapter 3 discusses details of the challenges caused for distance relays in the presence of CIRESs and also presents some scenarios in the test system where distance relays maloperate. The new proposed method is explained in Chapter 4. This method prevents the need to modify the relay design. Chapter 5 evaluates the performance of the proposed solution, and Chapter 6 concludes the paper.

Chapter 2

Test System

PSCAD/EMTDC simulations of the IEEE 9-bus system are used for this study. Detailed specifications of the modified system are presented in Fig. 2.1. As Fig. 2.1 shows, the SG at bus 9 of the original system is replaced by a 13.5-kV, 100-MVA CIRES that is interfaced with bus 9 through a 13.5/230-kV, 150-MVA transformer, denoted by T3. The HV side of T3 is considered to be the point of common coupling (PCC) for the CIRES. Since the fast dynamics of the source—either PV panels or Type IV wind turbines—are decoupled from the grid by the DC link capacitor, the source along with the source-side converter is modeled by a controllable DC current source. During steady state, CIRES generates its rated power at unity PF at PCC. The CIRES rides through the fault using a chopper circuit [14]. Distance relays R98 and R89 protect line L89. Zones 1 and 2 of R98 protect 90% and 120% of L89, respectively. The relays are modeled similar to a commercial relay with a quadrilateral characteristic [15]. The resistive reach of zone 1 is the same as the default value for this relay and equals 100 Ω. The same applies for the angle of the directional

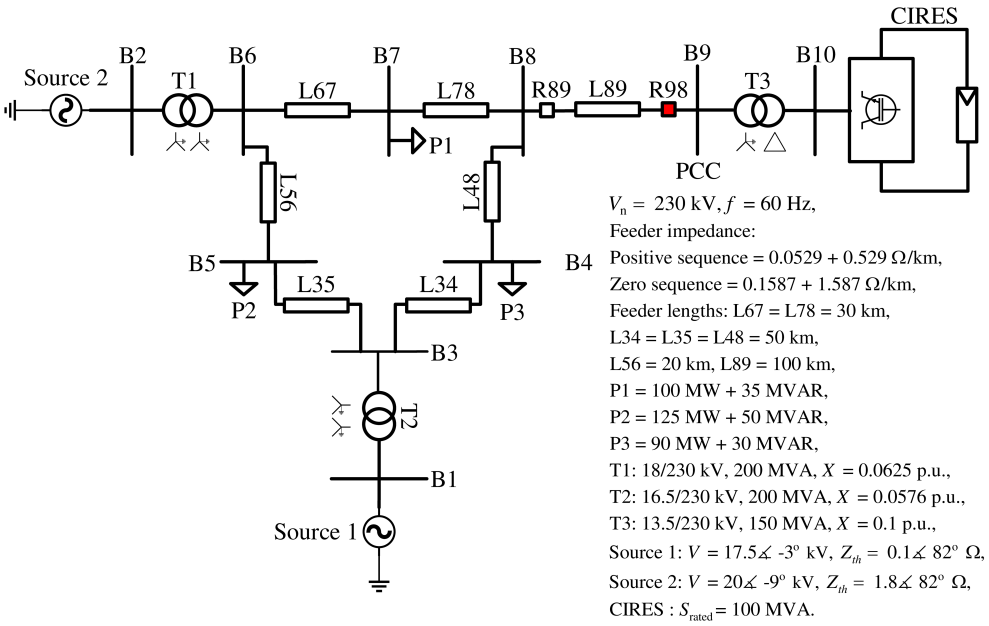

Figure 2.1: Diagram of the sample balanced power network operating in three phase mode.

element.

Chapter 3

Distance Protection Challenges

This chapter demonstrates the challenges faced by distance relays in the presence of CIRESs, and how existing measures fail or even worsen the relay performance.

3.1 Remote Infeed

A distance relay is expected to measure the positive-sequence impedance to the fault, Z_f^+. However, the relay's measurement deviates from Z_f^+ when infeed fault current flows at the remote end of the line and the fault includes resistance—which is often the case [16]. For example, Fig. 3.1 shows the circuit diagram of phases B and C during a phase-B-to-phase-C-to-ground (BCG) fault. In this circuit, R_f is the fault resistance, R_g is the ground resistance, and l and r denote local and remote end quantities measured by R98 and R89, respectively. Using Kirchhoff's voltage law (KVL), the impedance measured by BC element of R98 for a BCG fault on line L89 is expressed as:

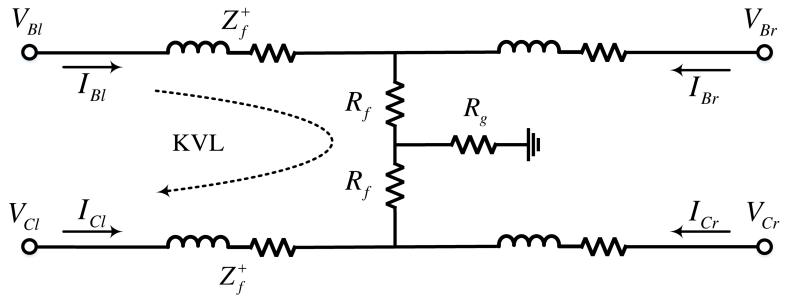

Figure 3.1: Circuit diagram of phases B and C during a BCG fault.

$$V_{Bl} - V_{Cl} = Z_f^+ I_{Bl} - Z_f^+ I_{Cl} + R_f(I_{Bl} + I_{Br}) - R_f(I_{Cl} + I_{Cr}) \tag{3.1}$$

$$Z_{BC} = \frac{V_{Bl} - V_{Cl}}{I_{Bl} - I_{Cl}} = Z_f^+ + R_f(1 + \underbrace{(\frac{I_{Br} - I_{Cr}}{I_{Bl} - I_{Cl}})}_{M_{r-BC}}) \tag{3.2}$$

Likewise, the impedance measured by the phase-A-to-ground (AG) element of R98 in Fig. 2.1 for an unbolted AG fault on line L89 is given by (3.3).

$$Z_{AG} = Z_f^+ + \underbrace{R_f(\frac{I_{Al} + I_{Ar}}{I_{Al} + KI_l^0})}_{M_{r-AG}} \tag{3.3}$$

I^0 is the zero-sequence current and K is the zero-sequence compensation factor. $R_f(1 + M_{r-BC})$ and $R_f M_{r-AG}$ in (3.2) and (3.3) are the fictitious impedances due to fault resistance and remote infeed current. When the system is supplied by only SGs, the angle between the fault currents at the two ends of the line is determined by the phase difference between the respective voltages. The voltage angles are relatively close, since large phase differences between the two end voltages of a line can put the system on the brink of instability. As a result, the angles of local and remote end currents are close. Therefore, the angles of the numerator and denominator of M_{r-BC} and M_{r-AG} are close, making $R_f(1 + M_{r-BC})$ and $R_f M_{r-AG}$ mainly resistive. For example, consider a

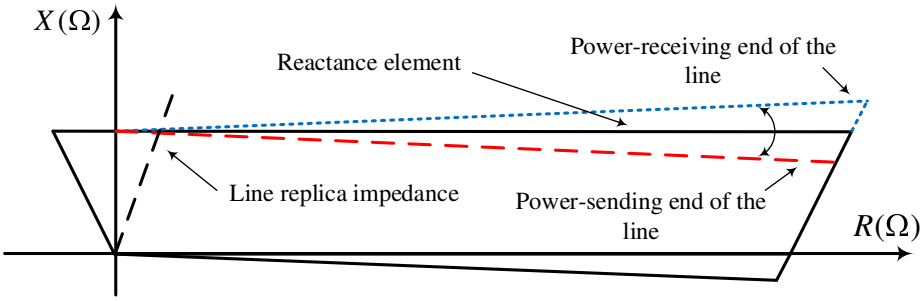

Figure 3.2: Tilting the reactance element of a distance relay.

scenario that the CIRES unit in the test system of Fig. 2.1 is replaced with an SG with the same rated power. If a BCG fault with a resistance of 20 Ω happens at 50% of line L89 from B9, the angles of the local currents of phases B and C are −174.4° and 60.4°, respectively. For the remote end currents measured by R89, these values are −177.7° and 40° for phases B and C, respectively. Hence, the angles of the numerator and denominator of M_{r-BC} is −157° and −146° respectively, resulting in an angle of −11° for M_{r-BC}. In this case, the reactance measured by R98 is 23 Ω, and the actual reactance to the fault is 21.2 Ω. Therefore, the measurements of R98 includes a small fictitious reactance added to the actual reactance to the fault. The effect of the small fictitious reactance added by these terms can be addressed easily by slightly tilting the reactance element in the clockwise and counterclockwise directions if the relay is at the power-sending and power-receiving end of the line, respectively (Fig. 3.2) [16].

In the presence of CIRESs, the angle between the two end currents is no longer entirely dependent on voltage angles. For example, in the system illustrated in Fig. 2.1, the equation for

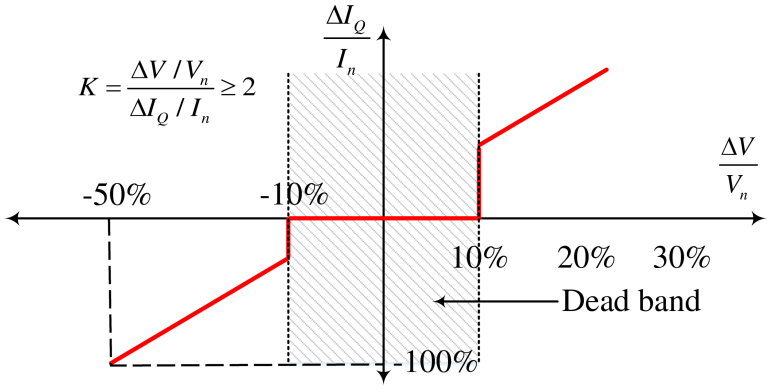

Figure 3.3: Reactive current requirement defined by the German GC for CIRESs.

the angle of the CIRES's current is expressed as:

$$I_l^+ = \sqrt{I_q^2 + I_d^2}\,\sin(\omega t + \mathrm{tg}^{-1}(\frac{I_q}{I_d}) + \theta_{v^+}) \tag{3.4}$$

in which I_d and I_q represent the two components of the CIRES's current in the synchronous reference frame, ω is the nominal angular frequency, and θ_{v^+} is the angle of the positive-sequence voltage. This current, which is the current measured by R98, is regulated by the control system of the CIRES at bus 9 such that the GC is satisfied.

Different GCs impose various requirements to ensure that sufficient reactive or active power is generated by the CIRESs over faults. GCs are categorized into two major groups namely European GCs (EU-GCs) and North-American GCs (NA-GCs). These GCs not only require the CIRESs to maintain their FRT capability but determine active and reactive power requirements that CIRES have to comply with during faulty conditions. As an example of EU-GCs, Fig. 3.3 shows the reactive current requirement defined by the German GC for RESs [17,18]. In this figure, V_n and I_n are the nominal voltage and current, respectively. ΔI_Q and ΔV are the superimposed

reactive current and voltage, respectively. This figure illustrates that for the CIRESs that comply with German GC, a voltage reduction of 10% results in an increase in generation of the reactive current. The ratio between the voltage reduction and reactive current generation should be greater than 2 in this GC. In contrast to the reactive current generation requirement of EU-GCs, a unity PF is often required by NA-GCs [19]. For both types of GCs, the angle of the local current for a relay at the substation of a CIRES can be substantially different from that of the remote end current. Accordingly, the fictitious impedances, $R_f(1+M_{r-BC})$ and $R_f M_{r-AG}$, can include a large imaginary part. Therefore, the effect of fault resistance and remote infeed current on the impedance measured by a distance relay is no longer primarily along the resistance axis. The fictitious reactance can cause considerable overreach and underreach, i.e. the relay measures a smaller or a larger impedance compared to the actual one to the fault, respectively. For the relays at the substation of CIRESs, this problem is aggravated by the small fault current magnitude of converters that limit the denominator of M_{r-BC} and M_{r-AG}, resulting in larger fictitious reactance.

For instance, consider a BCG fault at $t = 0.6$ s with a fault resistance of 20 Ω applied at 40% of line L89 from bus 9 in Fig. 2.1. The fault is in zone 1 of R98. Following [15], the reactance element of the quadrilateral characteristic is tilted 2° in the clockwise direction to address the effect of fault resistance and infeed currents. If the CIRES complies with EU-GCs, the nominal reactive current generated advances the angle of the local infeed current substantially beyond that of the remote infeed current. Thus, the numerator of M_{r-BC} leads the denominator by 57° in Fig. 3.4(a). Since the imaginary part of M_{r-BC} is significant—even larger than its real part—the impedance

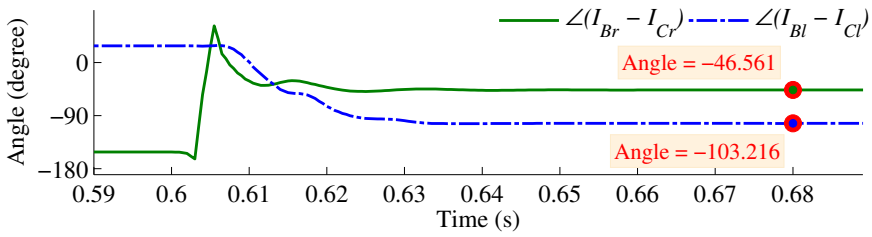

(a)

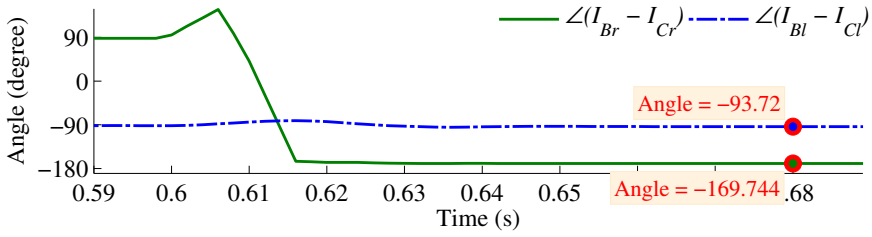

(b)

Figure 3.4: Angles of the numerator and denominator of M_{r-BC} during a BCG fault with $R_f = 20\ \Omega$ at 40% of line L89 from B9. (a) EU-GC. (b) NA-GC.

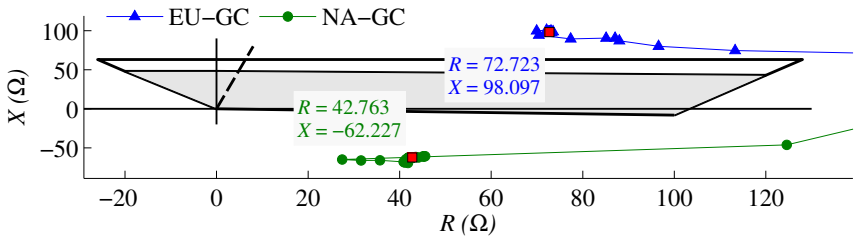

Figure 3.5: Impedances measured by R98 during a BCG fault with $R_f = 20\ \Omega$ at 40% of line L89 from B9.

measured by R98 in Fig. 3.5 is outside zone 1, and so the relay does not trip. On the other hand, if the CIRES complies with the unity PF requirement of the NA-GCs, the numerator of M_{r-BC} lags the denominator by 77° in Fig. 3.4(b). Therefore, as depicted in Fig. 3.5, R98 measures a negative reactance of about $-62\ \Omega$, which is in the fourth quadrant of the impedance plane, on which the quadrilateral characteristic is located, and outside zone 1. As a result, R98 falsely keeps the line in service. Similar failures can happen during other fault types as well.

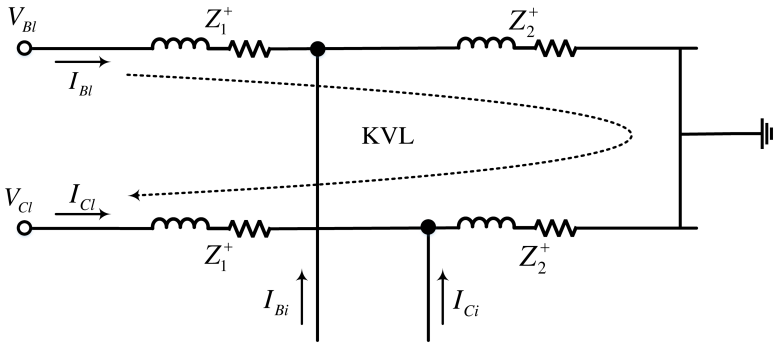

Figure 3.6: Circuit diagram of phases B and C during a BCG fault.

3.2 Intermediate Infeed

This section shows how a conceptually similar problem can be created for distance relays by intermediate infeed currents in the presence of CIRESs. In this respect, Fig. 3.6 shows the circuit diagram of a bolted BCG fault on line L48. The impedance measured by BC element of R98 during this fault can be obtained using KVL in this circuit.

$$V_{Bl} - V_{Cl} = Z_1^+(I_{Bl} - I_{Cl}) + Z_2^+(I_{Bl} + I_{Bi} - I_{Cl} - I_{Ci}) \tag{3.5}$$

$$Z_{BC} = \underbrace{Z_1^+ + Z_2^+}_{Z_f^+} + Z_2^+(\underbrace{\frac{I_{Bi} - I_{Ci}}{I_{Bl} - I_{Cl}}}_{M_{i-BC}}) \tag{3.6}$$

$$Z_{AG} = \underbrace{Z_1^+ + Z_2^+}_{Z_f^+} + Z_2^+(\underbrace{\frac{I_{Ai}}{I_{Al} + KI_l^0}}_{M_{i-AG}}) \tag{3.7}$$

Z_1^+ is the positive-sequence impedance of line L89, Z_2^+ is the positive-sequence impedance between bus 8–the intermediate infeed location–and the fault on line L48. Subscript i designates intermediate infeed quantities. When the system is supplied only by SGs, the phase difference between the intermediate infeed and local currents is determined by the phase difference

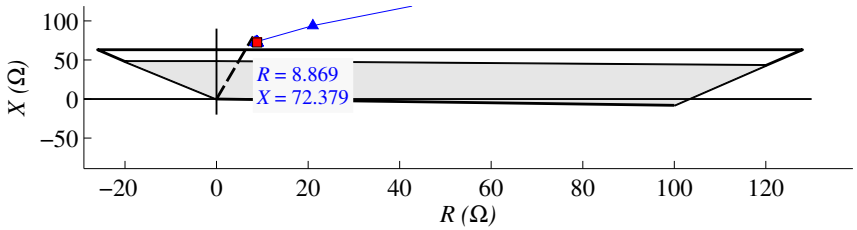

Figure 3.7: Impedance measured by R98 during a bolted BCG fault at 20 km of line L48 from B8 when the CIRES is replaced with an SG.

between their respective voltages. As discussed earlier, this phase difference is small, and so M_{i-BC} and M_{i-AG} are mainly real numbers. As a result, for conventional systems, the fictitious impedances $Z_2^+ M_{i-BC}$ and $Z_2^+ M_{i-AG}$ added to Z_f^+ are primarily along the line replica impedance, and the intermediate infeed is traditionally known to cause distance relays underreach. This issue is always taken into consideration for setting distance relays [16]. For instance, take the scenario where the CIRES is replaced with an SG and a bolted BCG fault happens at 20 km of line L48 from B8 in Fig. 2.1. For this fault, the angles of the local and intermediate infeed currents are $\measuredangle I_{Bl} = 172.2°$, $\measuredangle I_{Cl} = 35.2°$, $\measuredangle I_{Bi} = 161.7°$, and $\measuredangle I_{Ci} = 21.3°$. Therefore, $\measuredangle M_{i-BC} = -10°$, and R98 measures an impedance of $8.8 + 72.3\,j$, which is along the line replica impedance as shown in Fig. 3.7.

In the presence of CIRESs, however, the phase difference between local and intermediate infeed currents is no longer determined by the phase difference between pre-fault voltages. For instance, take two scenarios for a bolted BCG fault happening at $t = 0.6$ s at 20 km of line L48 from bus 8 in Fig. 2.1. Firstly, the CIRES complies to the EU-GC, and secondly the unity PF requirement of NA-GC is met. Fig. 3.8 shows the angles of the numerator and denominator of

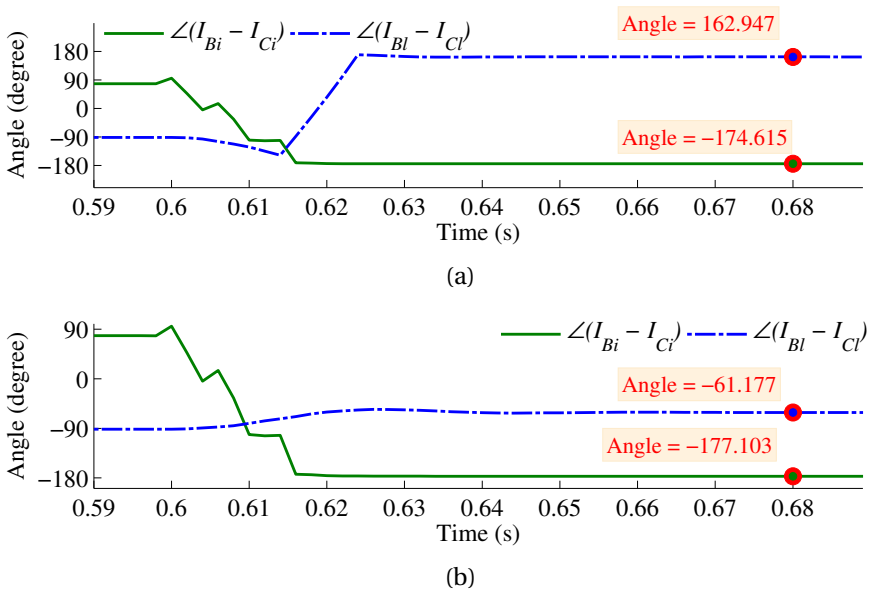

Figure 3.8: Angles of the numerator and denominator of M_{i-BC} during a bolted BCG fault at 20 km of line L48 from B8. (a) EU-GC. (b) NA-GC.

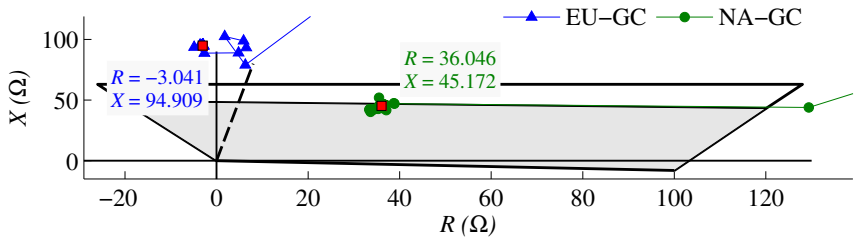

Figure 3.9: Impedances measured by R98 during a bolted BCG fault at 20 km of line L48 from B8.

M_{i-BC} during these two cases. Similar to the previous cases, GC compliance has increased the angle difference between the numerator and denominator of fictitious terms. For the case of EU-GC, M_{i-BC} has an angle of 22.4° in Fig. 3.8(a). This angle when added to 84.28° angle of Z_2^+ results in an angle of 106.6° for $Z_2^+ M_{i-BC}$ in (3.6), ending up in a large positive imaginary and a small negative real part for this term. Accordingly, as depicted in Fig. 3.9, R98 measures a larger reactance than the actual 63.48 Ω reactance to the fault along with a negative resistance that

shifts the measured impedance away from the line replica impedance. In the case of complying to NA-GC, the angle for M_{i-BC} decreases to about -116° in Fig. 3.8(b), which results in an angle of -31.72° for the fictitious impedance. Therefore, R98 measures a reactance equal to 45 Ω in Fig. 3.9, which is not only smaller than the actual one but inside the trip zone. These two cases clearly illustrate how R98 misoperates in the presence of intermediate infeed. If the fault moves further away from bus 8 or contains an amount of fault resistance, the error included in R98's measurements intensifies. Similar misoperations can happen for other fault types including SLG and LL too.

In this chapter, it was shown that how distance relays are prone to failure in the presence of remote and intermediate infeed currents. Existing measures used in conventional grids to address these failures such as tilting the reactance element fail in the presence of CIRESs. Solutions introduced in previous works mostly include changing the design of distance relays, while the solution proposed in the following chapter does not require such modification.

Chapter 4

Proposed Solution

This chapter presents a new current control scheme for CIRESs to prevent the problems discussed in the last chapter. First, the operation of the CIRES during faults is explained. Then, the strategy to find the proper angle for the CIRES's fault current is devised. Finally, the overall approach is discussed. The primary purpose of the proposed method would be to move the impedance measured by the relay inside its relevant zone, and as a further step, pave the way for the relay to measure a reactance as close as possible to the correct reactance to the fault.

4.1 CIRES's Fault Current

As stated earlier, the large phase difference between the infeed and CIRES fault currents can cause misoperation of distance relays. SGs dominate the remote and intermediate infeeed currents due to their high short circuit capacity. To decrease the phase difference between fault currents, the angle of the CIRES's fault current should become as close as possible to that of an

SG. By doing so, the fictitious impedance measured by R98 in Fig. 2.1 will be resistive, and the relay will operate correctly.

The control system of the CIRES that regulates the fault current angle along with the RLC filter of the converter are shown in Fig. 4.1 [20]. The voltages at the grid and converter side of the RLC filter are denoted by V_g and V_c, respectively. To decouple the converter from the grid-side disturbances, feedforward compensation of the grid voltage, shown by red arrows in Fig. 4.1, are applied to the output signals of PI controllers [20]. The feedforward compensation signal makes V_t replicate the non-idealities of V_g, including its imbalance. Hence, the voltage across the RLC filter remains balanced during faults. Consequently, the CIRES's current, which is directly related to the voltage across the filter, is also balanced; i.e. it is essentially a positive-sequence current. Therefore, as shown in Fig. 4.2, the negative- and zero-sequence circuits are open in the equivalent circuit of the test system of Fig. 2.1 for an AG fault on line L89. In this figure, Z_T, Z_{L1}, Z_{L2}, and Z_g are the impedance of transformer T3, the impedance from R98 to the fault location on line L89, the impedance from the fault to bus 8, and the equivalent Thevenin impedance of the system behind bus 8, respectively. For example, Fig. 4.3 shows the voltage and current waveforms measured at the low voltage (LV) side of transformer T3 in Fig. 2.1 during a phase-A-to-phase-B-to-ground (ABG) fault at $t = 0.6$ s with $R_f = 10\ \Omega$ at 30% of line L89 from B9. It can be seen that as soon as the fault happens, the voltage goes unbalanced; however, the current of the CIRES remains balanced.

As a result of the open circuit in the negative- and zero-sequence circuits, the only controllable variables that influence the fictitious impedance measured by R98 are the magnitude and

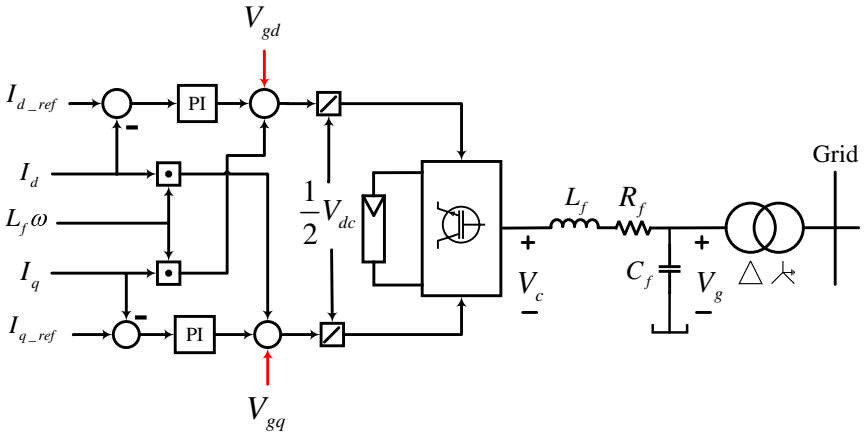

Figure 4.1: Control system of a CIRES.

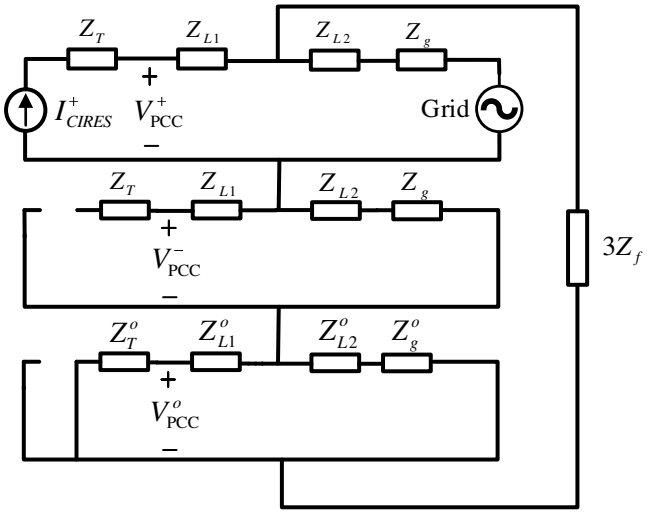

Figure 4.2: Equivalent sequence circuit of the test system during an SLG fault.

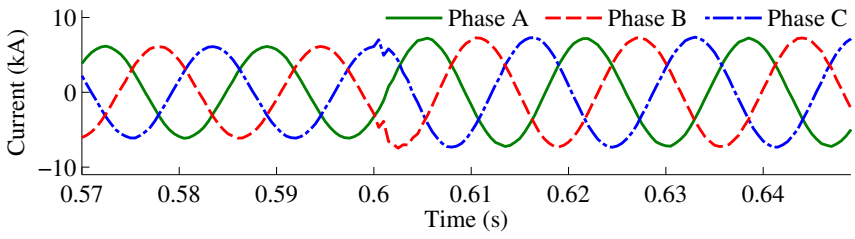

(a)

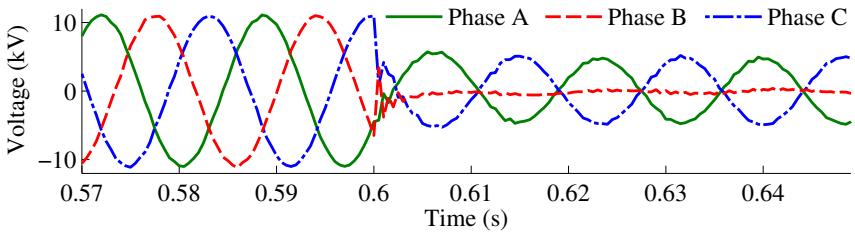

(b)

Figure 4.3: Measurements at LV side of T3 during a an ABG fault with R_f = 10 Ω at 30% of line L89 from B9. (a) Current. (b) Voltage.

angle of the positive-sequence component of the local current expressed in (3.4). This relation indicates that the current angle can be regulated through the I_q/I_d ratio. By means of proper references for I_d and I_q—denoted by I_{d_ref} and I_{q_ref}—as soon as a voltage-drop is detected, the angle of the local current can be regulated such that the phase difference between the fault currents of the CIRES and infeed decreases, and R98 measures an accurate reactance.

4.2 Selection of Reference Currents

The following formulates the strategies to choose proper I_{d_ref} and I_{q_ref} to meet the above objectives.

The phase angle between the negative- and positive-sequence currents generated by an SG during different types of asymmetrical faults follows the pattern shown in Fig. 4.4 [1]. This

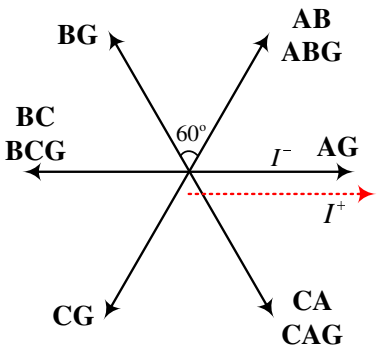

Figure 4.4: Phase relation between symmetrical components of SG's fault current [1].

pattern is used by existing relays to determine the fault type.

Through this pattern, the reference angle for the positive-sequence current of a CIRES such that it imitates the positive-sequence current angle of an SG can be found. Therefore, the phase difference between the local and infeed currents would be similar to the phase differences observed in conventional systems supplied only by SGs. As a result, the problems introduced by CIRES would be obviated.

To reach this goal, two challenges should be overcome. Firstly, the angle for I_l^- should be calculated, while there is no negative-sequence current present at relay location due to feedforward compensation. Secondly, the fault type should be identified. By knowing these two values, the proper angle for I_l^+ can be found using the pattern. The two following strategies formulate how to find the angle of I_l^-.

4.2.1 Replicating SG's current angles

One approach to circumvent the problem of not having any negative-sequence current in relay's measurements is to find the angle of I_l^- assuming that the CIRES is replaced by an SG. This approach is effective because the objective is to make $\measuredangle I_l^+$ of the CIRES also imitate that of an SG. If the CIRES is replaced by an SG, $\angle I_l^-$ is given by:

$$\angle I_l^- = \measuredangle V_{PCC}^- - \angle Z_{eq}^-. \tag{4.1}$$

In this equation, $\measuredangle V_{PCC}^-$ is the angle of the negative-sequence voltage at PCC, and $\angle Z_{eq}^-$ is the angle of the negative-sequence impedance of the transformer T3 in series with the negative-sequence impedance of the hypothetical SG. $\angle Z_{eq}^-$ can be chosen based on the typical values of an SG's impedance, e.g. 84° [21].

Using this method, the large phase difference between numerator and denominator of fictitious terms shrinks significantly and the relay operates fine.

4.2.2 Improved performance over SG emulation

Imitating the angle pattern of an SG decreases the angles of fictitious terms noticeably. However, it does not make it zero which is the perfect condition in which the fictitious impedance becomes completely resistive. To reach this perfect condition, the second approach for calculating the angle of the negative-sequence current is proposed here.

To make the angles of M_{r-BC} and M_{r-AG} zero, local and remote end negative-sequence currents should become in phase. Using the circuit depicted in Fig. 4.2, the angle of the remote

end negative-sequence current can be found using:

$$\angle I_l^- = \measuredangle V_{PCC}^- - \alpha \tag{4.2}$$

In this equation, α is the angle of the impedance resulted from series connection of Z_{L2} and Z_g. The problem here is that this angle alters as the fault location changes because Z_{L2} is the impedance from the fault to the end of line L89. To overcome this challenge, α is found for the worst fault scenario for which the distance relay is highly prone to maloperation that is a fault at the relay's reach point with the highest expected resistance. Given the large amount of R_f, even a small angle for M_{r-BC} or M_{r-AG} for such a scenario can change the fault zone determined by a distance relay. However, for other fault conditions, small angles for M_{r-BC} or M_{r-AG} do not significantly affect the zone of the measured impedance. Thus, if the CIRES's fault current is regulated such that the angles of M_{r-BC} and M_{r-AG} become zero for the worst fault condition, the relay can securely operate for other faults. The initial value for α can be set equal to the angle of Z_g, previously discussed. This stems from the fact that in Fig. 4.2, the angle of the remote end negative-sequence current, $\angle I_r^-$, roughly equals $\measuredangle V_{PCC}^- - \angle Z_g$ as Z_g is substantially larger than Z_{L2} for a reach point fault. As a result, since the objective is to make $\measuredangle M_{r-BC}$ and $\measuredangle M_{r-AG}$ zero, putting $\angle I_l^-$ equal to $\angle I_r^-$ by choosing $\angle Z_g$ as the initial value for α can give a good estimate of its final proper value. Then, the following iterative approach fine tunes α.

1. Model different fault types at the reach point with the highest expected resistance.

2. Calculate $\measuredangle M_{r-BC}$ and $\measuredangle M_{r-AG}$ for each fault type.

3. Add the $\measuredangle M_{r-BC}$ and $\measuredangle M_{r-AG}$ to α for the respective fault type.

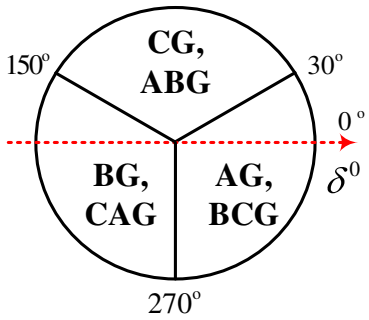

Figure 4.5: Angle zones used for fault type classification.

For R98 and line L89 in the test system of Fig. 2.1, α is 72° for line-to-line (LL) faults, 74° for line-to-line-to-ground (LLG) faults, and 63° for SLG faults. The maximum fault resistance considered to obtain these values for α is 100 Ω, which is the default fault resistance coverage of the quadrilateral characteristic of a commercial distance relay.

After finding $\angle I_l^-$ using (4.1) or (4.2), in order to find the reference angle for the CIRES's positive-sequence current through the pattern given in Fig. 4.4, the type of fault should also be identified. This can be achieved using the fault type classifier developed in [22]. This method determines the fault type within a few milliseconds by measuring the phase difference between the voltage sequence components and comparing them with the pattern shown in Fig. 4.5. In this figure, δ^0 is the phase lead of the negative-sequence voltage over the zero-sequence voltage. The two faults associated with each zone are distinguished based on the magnitude of phase voltages. This classifier can be used in both conventional grids as well as those containing CIRESs. Once the fault type and the expected angle of the negative-sequence current are identified, the reference angle for the CIRES's positive-sequence current can be generated using Fig. 4.4. To have the desired current angle at PCC, a simple closed-loop PI controller system is employed.

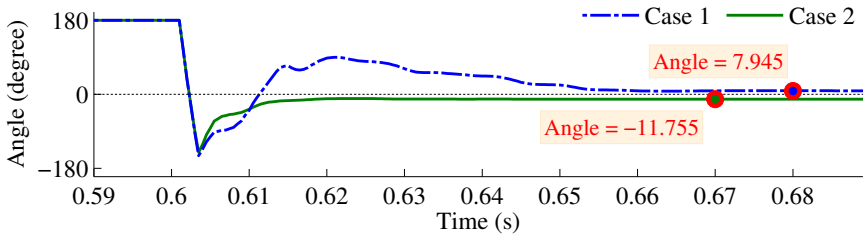

Figure 4.6: Angles of M_{r-BC} for cases 1 and 2.

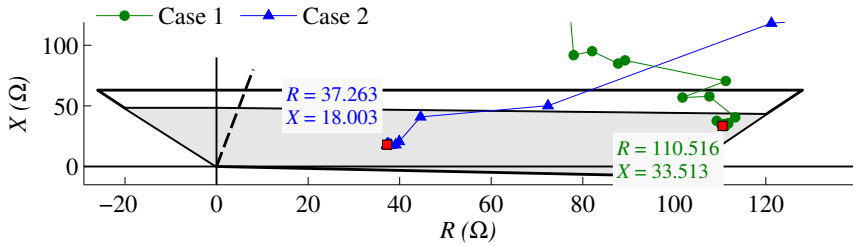

Figure 4.7: Impedances measured by R98 for cases 1 and 2.

The following two case studies exhibit the performance of the proposed method in regulating $\angle I_l^+$ of the CIRES using the first method such that the angle of an SG's fault current is emulated. These case studies are for the fault condition of Fig. 3.4. In case 1, the CIRES discussed in chapter 2 is connected to bus B10. In case 2, the CIRES is replaced by an SG with the same rated power. Fig. 4.6 depicts the operation of the proposed method for cases 1 and 2. The 57° and 76° angle differences between the numerator and denominator of M_{r-BC} observed in Fig. 3.4 has decreased to about 8° in Fig. 4.6 for case 1. This angle is even smaller than −11.75° observed for case 2 (Fig. 4.6). As a result, unlike Fig. 3.5, the impedance measured by R98 after the implementation of the proposed method lies within zone 1 in Fig. 4.7. It should be noted that the differences between the impedances measured for cases 1 and 2 in Fig. 4.7 are mainly due to different magnitudes of fault currents for CIRESs and SGs, resulting in different magnitudes for M_{r-BC}.

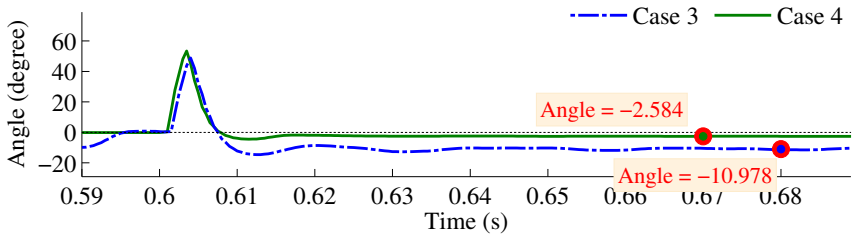

Figure 4.8: Angles of M_{r-AG} for cases 3 and 4.

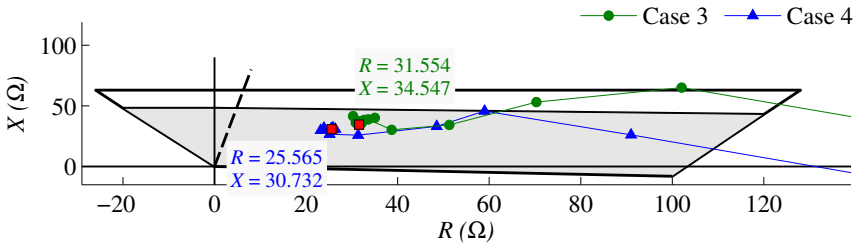

Figure 4.9: Impedances measured by R98 for cases 3 and 4.

To evaluate the performance of the proposed method for SLG faults, two more cases are defined. In case 3, the CIRES is in service, while in case 4, the CIRES is replaced by an SG similar to case 2. For both cases, an AG fault with $R_f = 20\ \Omega$ happens at 60% of line L89 from B8. Fig. 4.8 illustrates that the proposed method decreases the angle of M_{r-AG} such that it gets close to that of an SG, which is near zero. As a result, R98 operates properly and measures a reactance inside zone 1 with a difference of about 3 Ω with the actual reactance to the fault (Fig. 4.9).

By means of this approach, the phase difference between the local and infeed currents decreases, and the fault current angle of the CIRES is similar to that of an SG. Meanwhile, the limited fault current of the converter makes the CIRES a weak source. Therefore, conventional weak infeed tripping schemes, such as echo keying logic and weak infeed tripping logic, can be activated for R98 [15, 23, 24]. These schemes often require a communication link with minimal bandwidth between the relays at the two ends of the line.

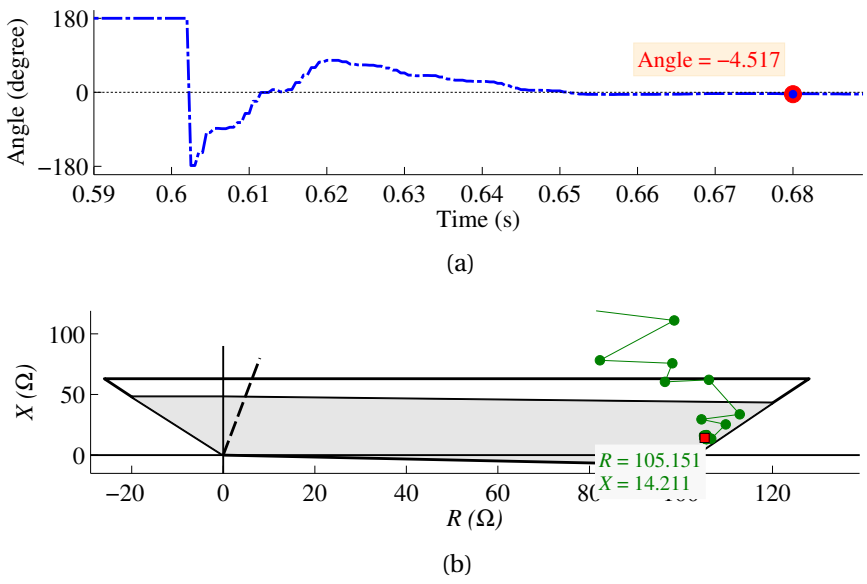

Figure 4.10: Results obtained for case 5. (a) $\measuredangle M_{r-BC}$. (b) Impedance measured by R98.

Two more case studies similar to cases 1 and 3, denoted by cases 5 and 6, evaluate the performance of the second method which uses (4.2) for calculating the angle of I_l^-. Fig. 4.10(a) displays the angle of $\measuredangle M_{r-BC}$ for case 5. It can be seen that using this method, $\measuredangle M_{r-BC}$ decreases to $-4.5°$, which is less than both of the angles observed in Fig. 4.6 for cases 1 and 2. Thus, as shown in Fig. 4.10(b), R98 measures an impedance inside the trip zone and closer to the actual 21 Ω impedance to the fault compared to case 1 (Fig. 4.7). For case 6, as Fig. 4.11(a) displays, the angle of M_{r-AG} decreases significantly compared to both cases 3 and 4 and becomes almost zero. Therefore, R98 measures the reactance with a difference of less than a Ohm with the actual value and inside the trip zone in Fig. 4.11(b).

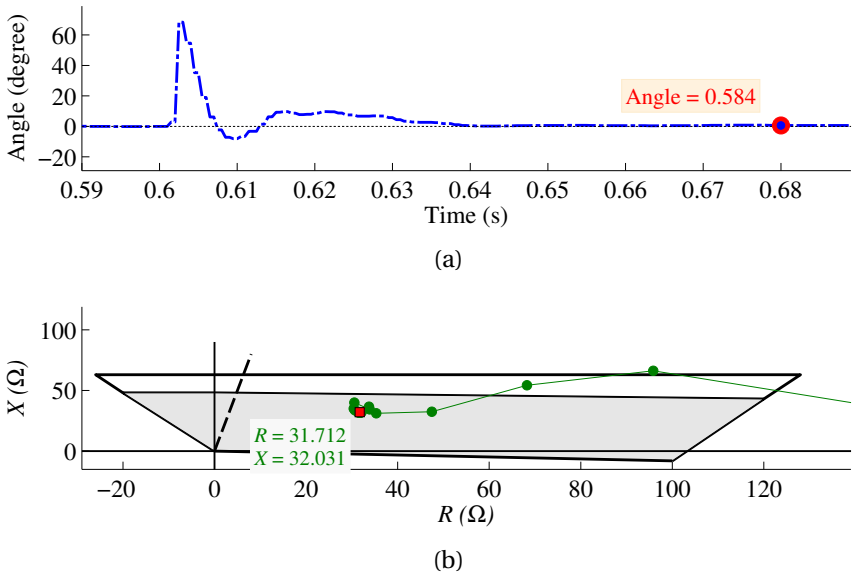

Figure 4.11: Results obtained for case 6. (a) $\measuredangle M_{r-AG}$. (b) Impedance measured by R98.

4.3 Overall Approach

The overall flowchart of the proposed method is plotted in Fig. 4.12. First, a disturbance detector (DD) similar to the DDs used by commercial relays is used for fault detection [24]. The second step is to identify the fault type using the pattern of Fig. 4.5 and the voltage level of each phase, as discussed earlier. These two steps can be taken within 2 to 3 ms. Then, the reference angle for the positive-sequence current can be calculated using (4.1) or (4.2) depending on the selected method. Afterwards, new current references, I_{d_ref} and I_{q_ref}, are generated and applied to the CIRES's control system.

Once the approach proposed in Section 4.2.2 is implemented, R98 can correctly differentiate between in-zone and out-of-zone faults close to its reach setting. Therefore, the reactance element does not need to be tilted. It should also be noted that for close-in faults, even a small

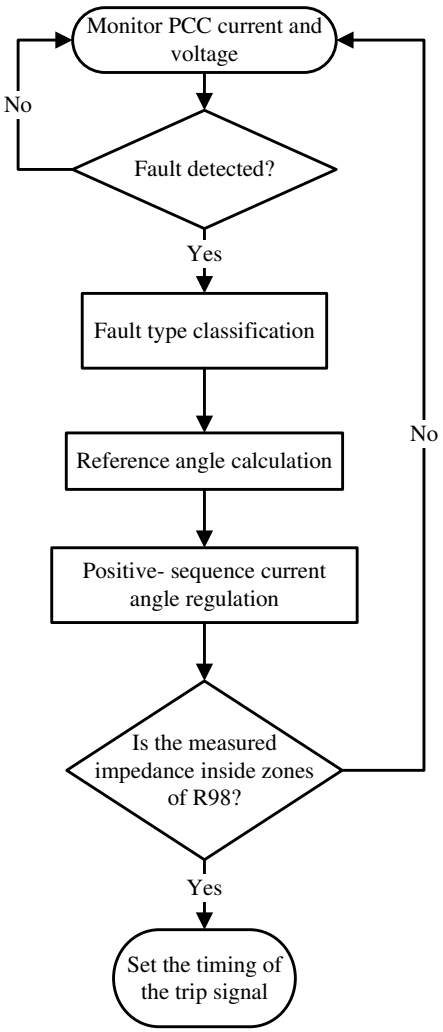

Figure 4.12: Flow of the proposed method.

negative angle for M_{r-BC} and M_{r-AG} might result in a non-negligible negative reactance if the fault resistance is huge, like 80 Ω or beyond. Therefore, it is suggested to set the angle of the directional element of the quadrilateral characteristic of R98 based on the reactance measured by the relay during a close-in high-resistance fault. These changes can be easily applied to the setting of existing commercial relays. Therefore, there will not be any need for designing new relays.

Chapter 5

Performance Evaluation

In addition to the cases presented in the previous chapter, some more cases are presented here which evaluate the performance of the solution proposed in Section 4.2.2. These cases include various scenarios in the test system of Fig. 2.1. The scenarios include different fault locations, fault resistances, and fault types. For the cases discussed in the following, the fault happens at t = 0.6 s, and the CIRES produces its rated power at unity PF before the fault.

5.1 Zone 1 Faults

5.1.1 Internal Faults

Table 5.1 reports measurements of R98 during different SLG, LLG, and LL faults on line L89 of Fig. 2.1. This table also includes the angles of M_{r-BC} and M_{r-AG}, generally denoted by $\measuredangle M_r$, and the actual reactance between the relay and the fault, denoted by $\hat{X}$. Fault resistances of 10 Ω, 50 Ω,

Table 5.1: R98 measurements during different faults on line L89

Fault type	R_f (Ω)	Distance from R98 (km)	$\angle M_r$ (°)	X (Ω)	R (Ω)	$\hat{X}$ (Ω)
AG	10	30	−0.57	15.75	13.13	15.87
		60	0.79	31.93	17.70	31.74
	50	30	−1.48	14.44	56.23	15.87
		60	−0.54	31.08	70.57	31.74
	90	30	−2.66	11.48	92.48	15.87
		60	−1.91	28	113.45	31.74
BCG	10	30	−5.72	11.43	55.62	15.87
		60	−3.82	28.19	66.54	31.74
	50	30	−1.61	11.07	217.25	15.87
		60	−3.17	21.49	237.32	31.74
	90	30	−0.79	12.77	330.9	15.87
		60	−2.83	20.67	316.95	31.74
BC	10	30	−6.17	13.43	29.17	15.87
		60	−3.93	29.84	35.75	31.74
	50	30	−6.16	5.04	126.92	15.87
		60	−3.97	23.36	146.56	31.74
	90	30	−6.06	−1.13	201.54	15.87
		60	−3.78	19.93	223.67	31.74

and 90 Ω represent low-resistance, medium-resistance, and high-resistance faults. Zone one of R98 covers the first 90% of L89, and so the reach setting of this zone is 48 Ω.

The 5th column of Table 5.1 indicates that for all scenarios, R98 measures a reactance inside zone 1 and trips instantaneously. In the case of AG faults, $\angle M_{r-AG}$ remains close to zero, and thus, the difference between the actual and measured reactance remains below 4 Ω. The 4 Ω difference between the actual and measured reactance corresponds to a fault at 30 km from R98 with R_f = 90 Ω. The angle of M_{r-AG} and the impedance measured by R98 for this fault are

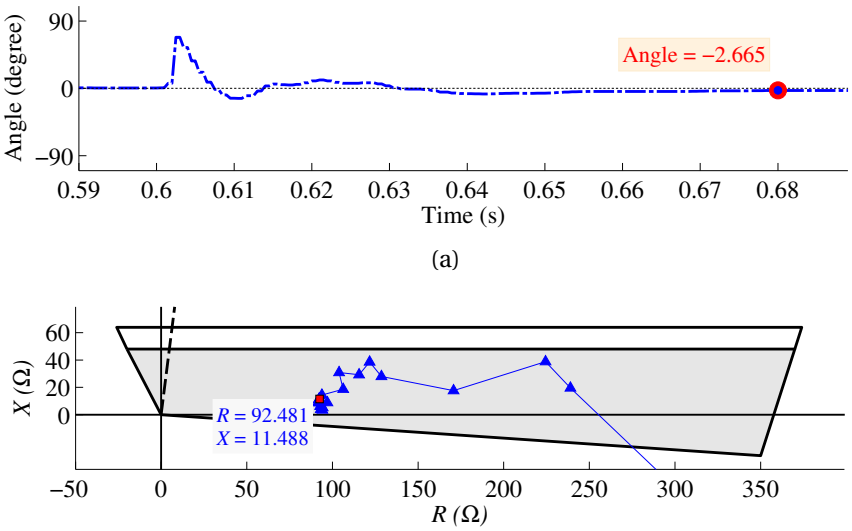

Figure 5.1: Results obtained during the AG fault at 30 km from R98 with R_f = 90 Ω reported in Table I. (a) $\angle M_{r-AG}$. (b) Impedance measured by R98.

depicted in Fig. 5.1. It is evident in Fig. 5.1(a) that the proposed method succeeds in regulating $\angle M_{r-AG}$ to about zero within a cycle after fault inception. As a result, the measured impedance enters zone 1 within 9 ms and remains in that zone for the entire duration of the fault (Fig. 5.1(b)). For BCG and BC faults, the results of Table 5.1 are very similar, confirming that the zero-sequence current flowing from the grounded HV side of T3 does not affect the angle of M_{r-BC}. During LL and LLG faults also the measured X is below the reach setting, and R98 operates correctly.

5.1.2 Faults at Reach Setting

To investigate the performance of the proposed method for the worst fault scenario, two faults including an AG and a BCG fault with R_f = 100 Ω were applied at 90% of L89 from B9. The faults are at the reach setting of R98 and the fault resistance is equal to the default resistance coverage

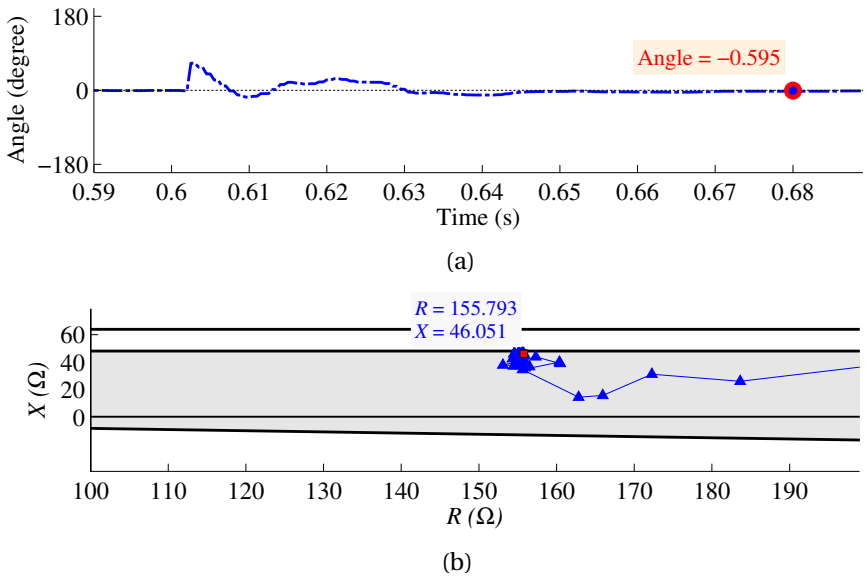

Figure 5.2: Results obtained during an AG fault with $R_f = 100\ \Omega$ at R98's reach point. (a) $\angle M_{r-AG}$. (b) Impedance measured by R98.

of a commercial relay. It can be observed in Figs. 5.3(a) and 5.2(a) that as a result of fine tuning α based on the method developed in Section 4.2.2, the angles of M_{r-AG} and M_{r-BC} drop to zero quickly after the onset of the fault. Consequently, as illustrated in Figs. 5.3(b) and 5.2(b), R98 measures an impedance inside zone 1 with a reactance equal to the reach setting. A large resistance is measured by R98, but it can be addressed by increasing the fault resistance coverage of the relay without impacting the relay performance. The fault resistance coverage in Figs. 5.3(b) and 5.2(b) is 375 Ω, which is substantially lower than $R = 520\ \Omega$, obtained during maximum local power transfer through line L89. These figures highlight desired performance of the proposed method for the worst fault scenario.

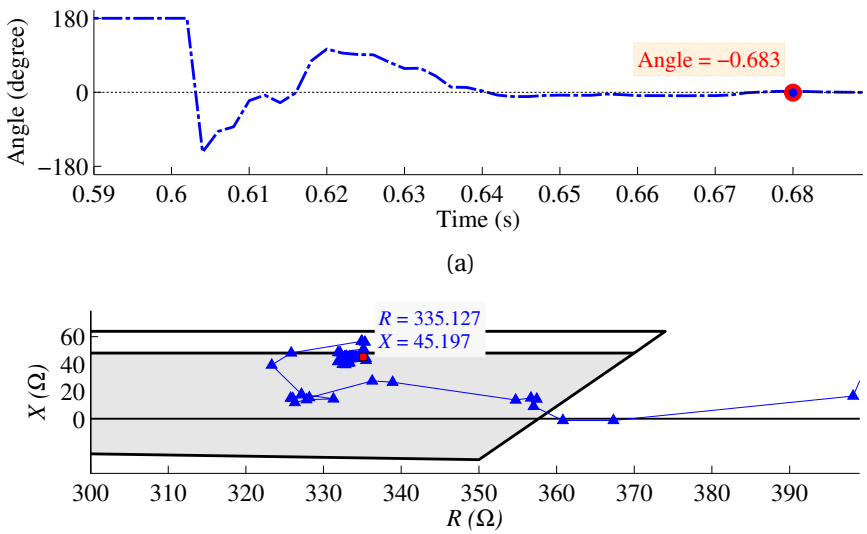

Figure 5.3: Results obtained during a BCG fault with $R_f = 100\ \Omega$ at R98's reach point. (a) $\measuredangle M_{r-BC}$. (b) Impedance measured by R98.

5.1.3 Close-In Fault

To further investigate the performance of the proposed method for close-in faults, a BC fault with $R_f = 30\ \Omega$ was applied on line L89 next to bus B9, where R98 is located. Fig. 5.4 shows the current and voltage waveforms during this fault condition. It is shown that the current maintains balanced after experiencing a transient of about a cycle. Compared to the current waveform observed in Fig. 4.3(a), in this condition, it takes a longer time for the transients to fade away. This can be attributed to the speed of the inverter's control system and the PI controllers as they try to regulate the current angle based on the provided references. Moreover, as displayed in Fig. 5.4(b), unlike the current, the voltage becomes unbalanced. As shown in Fig. 5.5, the measured impedance enters the trip zone quickly after the fault inception. Thus, R98 trips the line. For this fault, the angle of M_{r-BC} is $-7.7°$, as a result of which R98 measures a reactance that is slightly

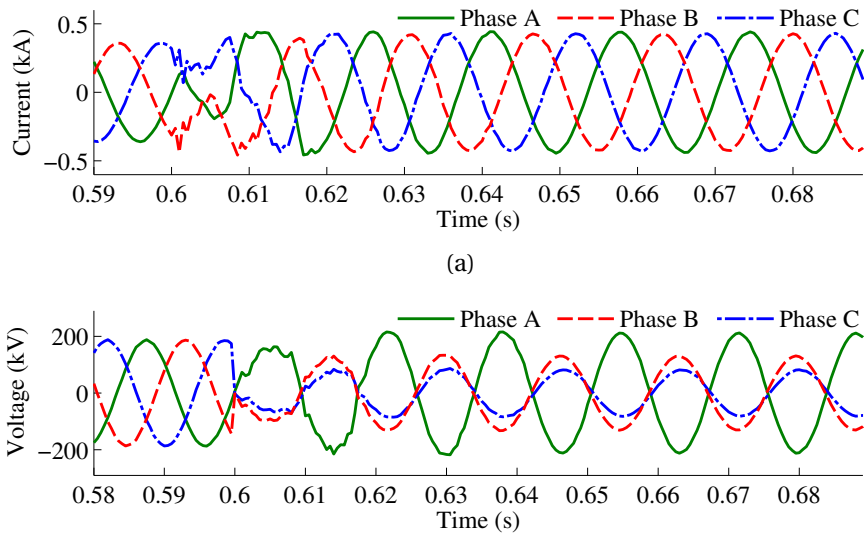

Figure 5.4: Measurements of R98 during a BC fault with $R_f = 30\ \Omega$ at PCC. (a) Current. (b) Voltage.

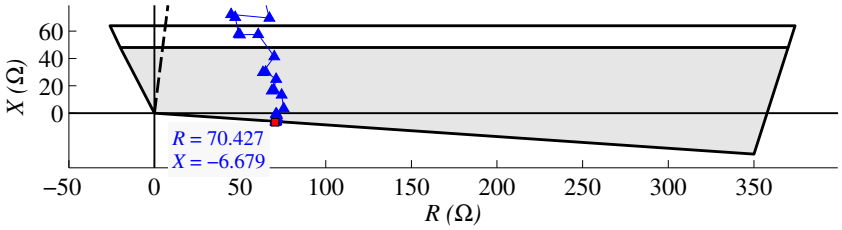

Figure 5.5: Impedance measured by R98 during a BC fault with $R_f = 30\ \Omega$ at PCC.

inside the fourth quadrant. Accordingly, as mentioned in Section 4.3, the angle of the directional element is chosen such that the impedance for such close-in faults lies within the zone.

As another example of close-in faults, an AG fault with $R_f = 100\ \Omega$ was applied at PCC. Fig. 5.6(a) illustrates that the final angle for the fictitious term is $-2.8°$. As the fault is far away from the reach point, the angle deviates from zero. Due to the negative angle for $\angle M_{r-AG}$ and the large fault resistance, R98 measures a negative reactance and inside the trip zone (Fig. 5.6(b)).

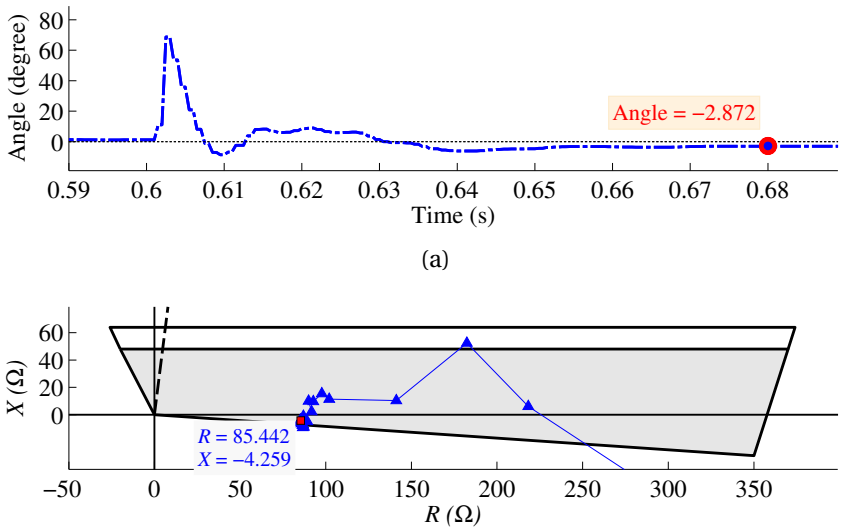

Figure 5.6: Results obtained during an AG fault with R_f = 100 Ω at PCC. (a) $\angle M_{r-AG}$. (b) Impedance measured by R98.

5.2 Zone 2 Faults

The performance of the proposed method was also verified for zone 2 faults. For example, consider a BCG fault with a resistance of 10 Ω at the remote end of L89 on bus B8. The second zone of R98 has a reach setting equal to 120% of the positive-sequence impedance of L89, i.e., 64 Ω. Fig. 5.7 depicts the impedances measured by R98 as the CIRES's control system tries to follow the reference currents generated by the proposed method, NA-GC, and EU-GC during this fault. This figure illustrates that using the proposed method, denoted by PM, the relay measures a reactance equal to 54.7 Ω, while the actual reactance to the fault is about 53 Ω, i.e. a difference of less than 2 Ω. On the other hand, when the CIRES sticks to unity PF as the requirement of NA-GC, R98 measures a negative reactance in the fourth quadrant with an error of about 73 Ω, which may

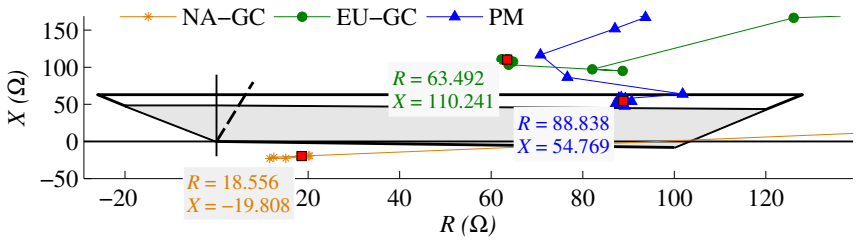

Figure 5.7: Impedances measured by R98 during a BCG fault with $R_f = 10\ \Omega$ on B8.

be mistakenly considered as a reverse fault by the relay. In the case of EU-GC, the CIRES increases its reactive current and decreases the active current that ends up in measuring a reactance with a difference of about 10 Ω with the actual one. Consequently, the relay maloperates in these two modes of operation. The obtained results demonstrate the effectiveness of the proposed method in paving the way for R98 to protect the whole length of feeder L89.

5.3 Intermediate Infeed Effect

To investigate the performance of the proposed method in the presence of intermediate infeed, the fault of Fig. 3.9 is modeled. As soon as the relay detects the fault inception, the fault type is identified using angle zones of Fig. 4.5. Next, the reference positive-sequence current angle is calculated using (4.2), and control system of CIRES tries to represent it at PCC. Consequently, as Fig. 5.8 indicates, the angle of M_{i-BC} decreases to about 5° which is much less than the 22° and −116° angles for this term observed in Fig. 3.8. As a result, unlike the misoperations observed in Fig. 3.9, R98 underreaches and measures an impedance close to the line replica impedance, similar to what traditionally happens in presence of SGs. Moreover, it should be borne in mind that the underreach level displayed in Fig. 5.9 increases as the fault resistance increases, which

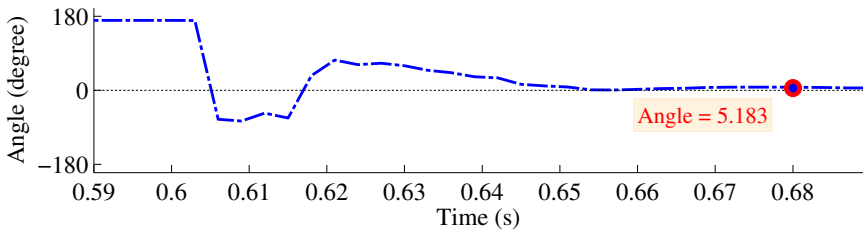

Figure 5.8: Angle of M_{i-BC} during the fault of Fig. 3.9

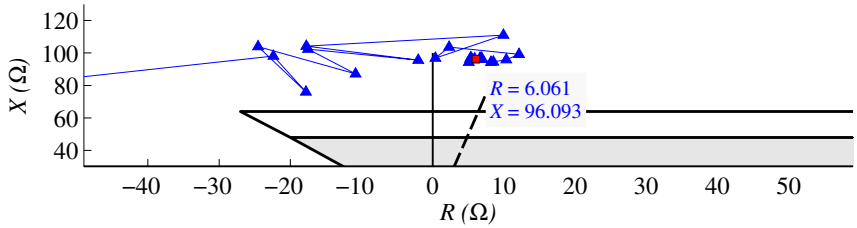

Figure 5.9: Impedance measured by R98 during the fault of Fig. 3.9

also helps keeping the measured impedance completely far from the first zone.

Chapter 6

Conclusion and future work

6.1 Summary

In this study, the effect of meeting modern GC's requirements on the performance of distance relays in close proximity of CIRESs was investigated. The studies were based on time-domain simulation of complete CIRES model and relaying algorithms using PSCAD/EMTDC program. It was shown that distance relays are prone to maloperation as the CIRES complies to modern GC's requirements. The cause of this maloperation was investigated and attributed to the angle difference between the local and the remote or intermediate infeed currents. In the grids mainly energized by SGs, this angle difference is small, thereby not affecting operation of distance relays noticeably. However, the angle difference can increase significantly in the presence of CIRESs. This happens because the CIRES's current angle is regulated by its control system and can have a large difference with the angle of the current at the other end of the line. Through

some case studies, it was shown that CIRES's compliance to NA- and EU-GCs can increase this angle difference such that the relay misoperates for both internal and external faults including some fault resistance. To address these maloperations, a new approach was proposed based on replicating SG's fault current angle at the CIRES's terminal. To this end, a new control scheme for the CIRES was proposed. This control scheme provides the references for the CIRES's control system such that the angle difference between the local and remote or intermediate infeed currents decreases. The references are generated using the negative-sequence voltage measured by the relay and the fault type classifier pattern used in commercial relays. Through several case studies, it was shown that using this method, distance relays in close proximity of CIRESs operate properly and in some cases even better than what traditionally happens in the presence of SGs. This method uses local variables and requires no communication infrastructure, thereby being cost-effective. In addition to the cost of the communication infrastructure, the cost difference between a distance and a line current differential relay, which is a significant number, should also be accounted toward cost savings of this method. This cost is important because the only two available relays for protection of a line emenating from a CIRES are line current differential and distance relays. If a distance relay, as the cheaper of the two, can be used as the primary relay, the protection system will cost much less. Moreover, unlike existing method, the proposed method does not require any modification of distance relays.

6.2 Considerations

To better understand scope of applications of the proposed method, the following should be taken into account:

1. Using the proposed method, the CIRES will ride the fault with its maximum capacity. However, GCs are violated, and the angle of the CIRES's current is regulated through the proposed method.

2. The proposed method does not address maloperation of distance relays in the presence of CIRESs during balanced faults.

3. This method can be applied only to renewable energy sources connected to the grid through a converter-based interface.

6.3 Future Works

Further research on this topic can be listed as:

1. Effect of CIRESs on line current differential relays. The performance of line current differential relays as another option besides distance relays for protecting lines connected to CIRESs should be investigated.

2. Increasing the speed of the proposed method. Newly developed high-speed distance relays operate within less than half a cycle. To make the proposed method compatible with these relays, the angle regulation speed should be enhanced. Some possible solutions can be employing stationary reference frame instead of the synchronous reference frame in the control system of

the CIRES which prevents the need for using a phase locked loop. Moreover, digital filters can be used to speed up the measurement process.

3. Investigating the performance of distance relays in the presence of CIRESs during unbolted faults in the presence of intermediate infeed. In this research work, the sole effect of intermediate infeed was investigated. However, if the fault at the neighboring line contains some resistance, both intermediate and remote infeeds add fictitious impedances to relay measurements, the effect of which should be analyzed.

4. Investigating the performance of the proposed method for other types of control systems. In some CIRESs, there exist another control loop that controls the negative-sequence current. The modifications needed such that the proposed method can be applied to these systems can also be an interesting topic for future works.

Bibliography

[1] D90^{Plus} *line distance protection system, instruction manual*, General Electric (GE), Canada, Mar. 2012. [Online]. Available: www.gedigitalenergy.com/products/manuals/d90plus/gek-113240b.pdf

[2] J. Glover, M. Sarma, and T. Overbye, *Power system analysis and design, fifth edition*. Cengage Learning, 2012, p. 379.

[3] J. Grainger and W. Stevenson, *Power system analysis*. McGraw Hill, 1994, p. 380.

[4] S. Horowitz and A. Phadke, *Power system Relaying, fourth edition*. Wiley, 2014, p. 1.

[5] A. Morales, X. Robe, M. Sala, P. Prats, C. Aguerri, and E. Torres, "Advanced grid requirements for the integration of wind farms into the Spanish transmission system," *IET Renew. Power Gen.*, vol. 2, no. 1, pp. 47–59, Mar. 2008.

[6] *Renewable energy facts*, Natural Resources Canada, Aug. 2018. [Online]. Available: https://www.nrcan.gc.ca/energy/facts/renewable-energy/20069

[7] A. Hooshyar, M. A. Azzouz, and E. F. El-Saadany, "Distance protection of lines emanating from full-scale converter-interfaced renewable energy power plants–part I: Problem statement," *IEEE Trans. Power Del.*, vol. 30, no. 4, pp. 1770–1780, Aug. 2015.

[8] B. Chen, A. Shrestha, F. A. Ituzaro, and N. Fischer, "Addressing protection challenges associated with type 3 and type 4 wind turbine generators," in *2015 68th Annu. Conf. for Protective Relay Eng.*, Mar. 2015, pp. 335–344.

[9] A. Hooshyar, M. A. Azzouz, and E. F. El-Saadany, "Distance protection of lines emanating from full-scale converter-interfaced renewable energy power plants–part II: Solution description and evaluation," *IEEE Trans. Power Del.*, vol. 30, no. 4, pp. 1781–1791, Aug. 2015.

[10] A. Timbus, M. Liserre, R. Teodorescu, P. Rodriguez, and F. Blaabjerg, "Evaluation of current controllers for distributed power generation systems," *IEEE Trans. Power Electron.*, vol. 24, no. 3, pp. 654–664, Mar. 2009.

[11] *IEEE Guide for Protective Relay Applications to Transmission Lines*, IEEE Std. C37.113-1999, 1999.

[12] *Instruction Manual: SEL-411L relay, advanced line differential protection, automation, and control system*, SEL, USA, Feb. 2018. [Online]. Available: https://selinc.com/products/411L/

[13] K. Zimmerman and D. Costello, "A practical approach to line current differential testing," in *66th Annu. Conf. for Protective Relay Eng.*, May 2013, pp. 20 151 125–091 718.

[14] J. Conroy and R. W. Watson, "Low-voltage ride-through of a full converter wind turbine with permanent magnet generator," *IET Renew. Power Gen.*, vol. 1, no. 3, pp. 182–189, Sep. 2007.

[15] *Application manual for line distance protection REL670*, ABB, May 2017, version 2.2 ANSI. [Online]. Available: http://new.abb.com/substation-automation/products/protection-control/line-distance-protection/rel670

[16] G. Ziegler, *Numerical Distance Protection: Principles and Applications*. Publicis, 2011.

[17] M. Tsili and S. Papathanassiou, "A review of grid code technical requirements for wind farms," *IET Renew. Power Gen.*, vol. 3, no. 3, pp. 308–332, Sep. 2009.

[18] H. Berndt, M. Hermann, H. D. Kreye, R. Reinisch, U. Scherer, and J. Vanzetta, "Transmission code 2007 network and system rules of the german transmission system operators," Aug. 2007.

[19] M. P. LeBlanc, L. Evans, P. Gardner, and N. C. Scott, "Canadian grid code for wind development-review and recommendations," Garrad Hassan and CANWEA, Ottawa, Tech. Rep., 2005.

[20] A. Yazdani and R. Iravani, *Voltage-sourced converters in power systems: modeling, control, and applications*. John Wiley & Sons, 2010, p. 220.

[21] N. Tleis, *Power systems modeling and fault analysis*. Elsevier, 2008, pp. 609.

[22] A. Hooshyar, E. F. El-Saadany, and M. Sanaye-Pasand, "Fault type classification in microgrids including photovoltaic DGs," *IEEE Trans. Smart Grid*, vol. 7, no. 5, pp. 2218–2229, Sep. 2016.

[23] *IEEE Guide for Protective Relay Applications to Transmission Lines*, IEEE Std. C37.113-2015, 2015.

[24] *Instruction Manual for SEL-411L Relay*, SEL, Pullman, WA, USA, Jun. 2013. [Online]. Available: www.selinc.com/SEL-411L